Fuel 375 (2024) 132628

Contents lists available at ScienceDirect

Fuel

journal homepage: www.elsevier.com/locate/fuel

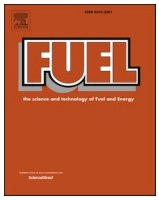

Full Length Article

# Atomistic insights into two-stage combustion of a single boron nanoparticle via reactive molecular dynamics

Muye Feng [a], Yi Wang [b], Dingyu Hou [c], Heping Li [d], Kai H. Luo [b,e,*], Xuefei Xu [b,*]

[a] School of Mechanical and Power Engineering, Nanjing Tech University, Nanjing 211816, China
[b] Center for Combustion Energy, Key Laboratory of Thermal Science and Power Engineering of Ministry of Education, Department of Energy and Power Engineering, Tsinghua University, Beijing 100084, China
[c] Beijing National Laboratory for Molecular Sciences, State Key Laboratory of Polymer Physics and Chemistry, Institute of Chemistry, Chinese Academy of Sciences, Beijing 100190, China
[d] School of Science, Hangzhou Dianzi University, Hangzhou 310018, China
[e] Department of Mechanical Engineering, University College London, Torrington Place, London WC1E 7JE, UK

ARTICLE INFO

*Keywords:*
Boron nanoparticle
Two-stage combustion
Molecular dynamics
Reactive force field

ABSTRACT

Boron (B) is a promising energetic additive for high-energy fuels, but its poor ignition and combustion characteristics limit its application in practical systems. The nano-sized B could alleviate these problems to a large extent. In this study, a reactive molecular dynamics simulation method is employed to investigate the fundamental combustion mechanisms of a single B nanoparticle (BNP). The experimentally observed two-stage combustion is reproduced. Moreover, the first stage is further divided into the pre-heating stage and the fast evaporation stage. The second stage is dominated by the B core combustion, during which a dynamic equilibrium of the interfacial layer and the oxide/evaporation layer is reached and drives the reaction. The diffusion mechanism of the BNP combustion is revealed. The evaporation of oxides and diffusion of ambient oxygen species into the oxide/evaporation layer proceed simultaneously during the fast evaporation stage. No ambient oxygen species diffuse into the B core but the diffusion of the core B atoms into the oxide/evaporation layer occurs throughout the simulation. Additionally, the diffusion of the core B atoms is enhanced with the rising temperature. Consistent with experimental results, $BO_2$ is found to be a dominant intermediate species during the combustion. Furthermore, our new finding is that $B_3O_4$ is also an important intermediate, which bridges the conversion of larger $B_xO_y$ species to the main combustion product $B_2O_3$. The new atomistic insights obtained from the present research could potentially benefit the design and practical application of nano-sized B as additives for high-energy fuels.

## 1. Introduction

Boron (B) is a promising additive for solid propellants and liquid fuels due to its exceptionally high gravimetric and volumetric heating values (58 kJ/g and 136 kJ/cm$^3$), which are superior to hydrocarbons and most metals, and therefore has attracted substantial research interests since 1960s [1,2]. However, its poor ignition and combustion characteristics make it still challenging to realize its full potential in practical applications. To date, the majority of research on the combustion of B considered the micron-sized particles. Recent advance in nanotechnology promotes the development of energetic nanoparticles as additives for high-energy fuels. As a result, investigation into ignition and combustion characteristics of nano-sized B has drawn much attention in the past decade [3–6]. In order to make full use of the highly energetic nano-sized B, understanding of the physical and chemical processes of its combustion is of great fundamental and practical importance.

Macek and Semple [7] carried out a pioneering study on combustion of B particles, in which they proposed the two-stage combustion of B. The first stage describes the particle burning while it is still coated with an oxide layer; the second stage involves the combustion of bare B, which begins after the oxide layer is completely removed by evaporation. The formation of the $B_2O_3$ oxide layer with a relatively high boiling point (2133 K [8]) and the extremely high melting and boiling temperatures of B (2348 and 4273 K, respectively [8]) lead to the difficulties in ignition and combustion of B. Subsequently, various models were

* Corresponding authors.
*E-mail addresses:* k.luo@ucl.ac.uk (K.H. Luo), xuxuefei@tsinghua.edu.cn (X. Xu).

https://doi.org/10.1016/j.fuel.2024.132628
Received 14 May 2024; Received in revised form 17 July 2024; Accepted 26 July 2024
Available online 1 August 2024

developed to understand the complex B combustion. King [9] assumed that the oxygen diffuses across the oxide layer to the B-$B_2O_3$ interface, whereas Glassman et al. [10] claimed that the boron diffuses through the oxide layer to the boron oxide-gas interface. It was concluded by Yeh and Kuo [2] that the diffusion of dissolved boron into molten $B_2O_3$ is much more dominant than the diffusion of gaseous $O_2$ through the $B_2O_3$ at elevated temperatures. Recently, Liang et al. [11,12] confirmed a bidirectional diffusion mechanism of both B and $O_2$ in the liquid $B_2O_3$.

The two-stage phenomenon was also observed during the combustion of nano-sized B [3–5], and the ignition and combustion characteristics of nano-sized B are found to be better than those of micron-sized B [3]. However, the emphasis of experimental studies [3–5] was mainly on the overall effects of temperature, pressure, and oxygen concentration on combustion performance of nano-sized B including ignition delay and burning times, leaving detailed mechanisms unclear, due to the limited understanding of the microscopic process. Wang et al. [13] conducted a molecular dynamics study on oxidation of a B nanocluster but they only focused on the low-temperature initial oxidation reactions and formation of the oxide layer. The microscopic mechanism of combustion of nano-sized B is still lacking but highly desirable. In this study, the reactive molecular dynamics simulation method is employed to investigate the fundamental combustion mechanisms of a single B nanoparticle (BNP). At the atomic level, we scrutinize the two-stage combustion of the BNP and reveal the associated diffusion mechanism. In addition, the gas phase and surface reactions are also studied in detail. Based on our atomic level observations, an improved understanding of the BNP combustion process is obtained.

## 2. Methods

### 2.1. ReaxFF reactive force field molecular dynamics

The ReaxFF is a bond-order based reactive force field, whose parameters are trained against quantum mechanics (QM) data. The ReaxFF molecular dynamics (MD) is able to describe the dissociation, transition, and formation of chemical bonds that cannot be achieved by MD simulation using non-reactive classic force fields. In addition, it undercuts the prohibitive computational cost of QM-based methods but reproduces a comparable level of accuracy thereby providing an affordable and powerful simulation approach for studying the long-time large-scale reactive systems. ReaxFF bond orders as shown in Eq. (1) are calculated directly from interatomic distances and continually updated at every time step to enable connectivity changes during the simulation [14].

$$\begin{aligned} \mathrm{BO}_{ij} &= \mathrm{BO}_{ij}^{\sigma} + \mathrm{BO}_{ij}^{\pi} + \mathrm{BO}_{ij}^{\pi\pi} \\ &= \exp\left[p_{bo1}\left(r_{ij}/r_o^{\sigma}\right)^{p_{bo2}}\right] + \exp\left[p_{bo3}\left(r_{ij}/r_o^{\pi}\right)^{p_{bo4}}\right] + \exp\left[p_{bo5}\left(r_{ij}/r_o^{\pi\pi}\right)^{p_{bo6}}\right] \end{aligned} \quad (1)$$

where BO is the bond order between atoms $i$ and $j$, $r_{ij}$ is interatomic distance, $r_o$ terms are equilibrium bond lengths, and $p_{bo}$ terms are empirical parameters. $\sigma$, $\pi$, and $\pi\pi$ denote the sigma bonds, pi bonds, and double pi bonds, respectively. The general expression of various energy components contributing to the ReaxFF potential is shown in Eq. (2) [15]:

$$E_{\mathrm{system}} = E_{\mathrm{bond}} + E_{\mathrm{over}} + E_{\mathrm{under}} + E_{\mathrm{lp}} + E_{\mathrm{val}} + E_{\mathrm{tor}} + E_{\mathrm{vdWaals}} + E_{\mathrm{Coulomb}} \quad (2)$$

where $E_{\mathrm{system}}$, $E_{\mathrm{bond}}$, $E_{\mathrm{over}}$, $E_{\mathrm{under}}$, $E_{\mathrm{lp}}$, $E_{\mathrm{val}}$, $E_{\mathrm{tor}}$, $E_{\mathrm{vdWaals}}$, and $E_{\mathrm{Coulomb}}$ represent total energy, bond energy, overcoordination energy penalty, undercoordination stability, lone pair energy, valence angle energy, torsion angle energy, van der Waals energy, and Coulomb energy, respectively. The energy terms in the ReaxFF force field are computed for every pair of atoms as a function of their interatomic distance or bond order.

More detailed information on exhaustive formulation of ReaxFF and its development can be found in previous articles [14,15]. ReaxFF MD methodology is particularly popular in the combustion-related research in the past decade [16–19] and has proven its effectiveness and powerfulness for studying the combustion of various nanoparticles [20–23].

### 2.2. Simulation details

LAMMPS package [24] is used to perform all of the ReaxFF MD simulations. The parameter set for B/O interactions, which has proven to be able to accurately describe the oxidation reactions of B clusters [25], is chosen as a suitable force field for the present study. The simulation procedure consists of two main parts: (1) nanoparticle construction under the canonical (NVT) ensemble, and (2) combustion reaction simulations under the combined microcanonical (NVE) and NVT ensembles, which will be introduced in detail in the following paragraphs. Four independent runs are carried out for the final combustion simulation system, and the results are averaged for analysis. The total simulation time of each run is 1.6 ns. Error bars (color filling around the curve) shown in figures are determined by the standard error of the mean. The time step used for simulations is 0.2 fs, and all results of production runs are recorded every 0.2 ps. A commonly used 0.3 bond order cutoff is employed to obtain the bonding information. The simulation results are visualized using OVITO [26].

The amorphous B is considered as a more feasible candidate for practical applications since its ignition and combustion characteristics are better than those of crystalline B [27], and thus is adopted in the present study. Due to the existence of an oxide layer on the B surface, we first build a core–shell B-$B_2O_3$ structure. Although experimental results showed that the $B_2O_3$ oxide layer covering the amorphous B has a certain degree of crystalline structure, the majority of the particle is generally of amorphous nature [2,28]. As a result, both core B and shell $B_2O_3$ structures are made amorphous during the process of nanoparticle construction. The detailed core–shell model is prepared following these steps: (1a) cut a 7 nm diameter $\alpha$-B nanoparticle from the crystalline structure; (1b) create the amorphous B (see XRD results in Fig. S1 in the Supplementary Material) by annealing the $\alpha$-B nanoparticle for 100 ps (heated up to 2800 K); (1c) cut the 6 nm diameter core from the annealed B nanoparticle; (2a) cut a 10 nm diameter $\alpha$-$B_2O_3$ nanoparticle from the crystalline structure; (2b) create the amorphous $B_2O_3$ (see XRD results in Fig. S2 in the Supplementary Material) by annealing the $\alpha$-$B_2O_3$ nanoparticle for 100 ps (heated up to 1100 K); (2c) cut a 1 nm thickness shell from the annealed $B_2O_3$ nanoparticle (radius from 3 to 4 nm); (3) combine the B core and the $B_2O_3$ shell together and then relax the core–shell structure at 300 K for 100 ps (denoted as BNP, see Fig. 1a). The BNP contains 19,961 atoms. All of the annealing and relaxation processes are performed under the NVT ensemble. After the relaxation, a thin B/$B_2O_3$ interfacial layer is observed, which will be studied in detail during the combustion reaction.

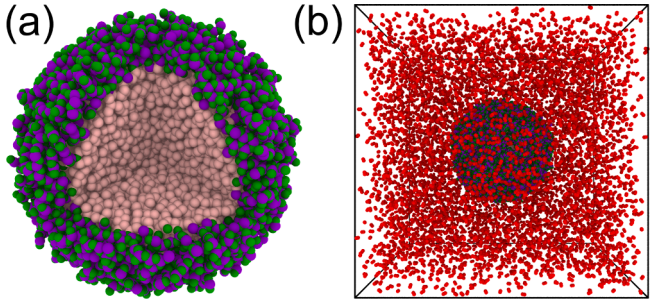


**Fig. 1.** Illustration of the nanoparticle structure and the simulation system: (a) three-dimensional view of BNP (relaxed core–shell B-$B_2O_3$ structure); (b) combustion simulation system. Atoms colouring scheme: core B – pink; shell B – purple; shell O – green; molecular oxygen O – red. (For interpretation of the references to color in this figure legend, the reader is referred to the web version of this article.)

Next, the prepared BNP is positioned at the centre of a 180 Å × 180 Å × 180 Å periodic simulation box filled with 7637 oxygen molecules (see Fig. 1b), the number of which is enough for complete combustion. In total, the combustion simulation system constructed for BNP contains 35,235 atoms. The centre of mass of BNP is kept at the centre of the box during the simulation. To heat the BNP from normal temperature, the initial temperature of the BNP is set as 300 K. Based on the high melting and boiling points of B and $B_2O_3$ mentioned in Introduction, 3000 K is chosen as an appropriate initial temperature for the ambient oxygen molecules and is kept constant as the environmental temperature for the combustion simulation. Our initial tests adopting simple NVE ensemble show that the reaction proceeds extremely slowly thus the simulation is computationally too expensive and time-consuming. Instead, we employ a strategy of combined NVE and NVT ensembles to study the combustion reactions. Specifically, the central spherical region with a specific radius of the simulation box is maintained under the NVE ensemble, while the temperature of the region outside the central sphere is kept constant at 3000 K under the NVT ensemble. The radius of the central NVE sphere is 5 nm, which is 1 nm larger than the designed radius of BNP considering any size change during the relaxation process. This strategy is designed to heat the BNP constantly in a hot environment, making the combustion simulation much more efficient.

## 3. Results and discussion

### 3.1. Two-stage combustion of BNP

A two-stage combustion phenomenon, which was observed experimentally during the combustion of both micron- and nano-sized B [2–4], is reproduced in the present study. The whole BNP is divided into three parts, namely, the B core, the interfacial layer, and the oxide/evaporation layer. The naming of the oxide/evaporation layer is inspired by our MD observation that will be explained later. We distinguish the three different parts using the radial number density profiles of O atoms in the system, the details of which are provided in Fig. S3 in the Supplementary Material. Accordingly, time evolution of diameter ($d$) or thickness ($t$) of different parts of BNP as well as of the whole BNP is obtained as shown in Fig. 2. By classifying the atoms, the temperature ($T$) of each part is determined based on the atomic kinetic energy, and the weight ($W$) of BNP is calculated using the numbers of B and O atoms of the BNP. Fig. 3 depicts the various temperature profiles and the weight loss curve of the BNP. The two stages of the previous combustion model are bounded by the complete removal of the oxide layer by evaporation when the combustion of bare B begins. However, at the atomic level, it is found that the oxide layer is not completely evaporated when the core combustion initiates and there is always a thin oxide layer, which keeps evaporating during the second stage (Stage II). This is the origin of the naming of the oxide/evaporation layer. Additionally, the first stage can be further divided into two sub-stages (Stages Ia and Ib). The first two time points at which the derivative of time evolution of $t_{oxide/evaporation}$ is zero are employed to distinguish the Stages Ia and Ib (at 0.21 ns), and Stages I and II (at 0.59 ns), respectively (see Fig. S4 in the Supplementary Material).

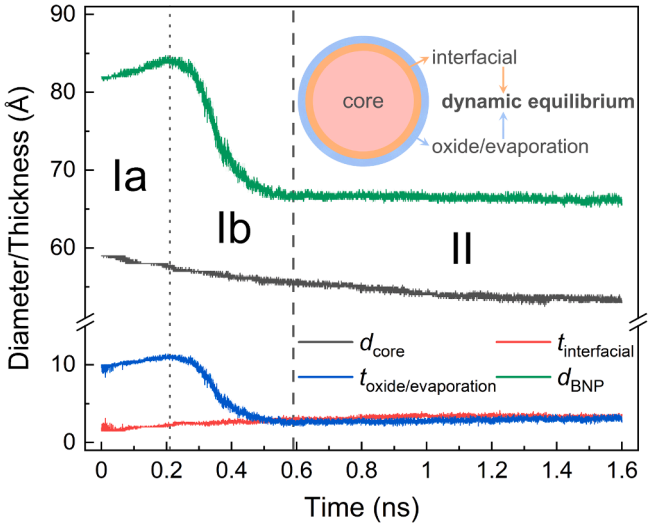


**Fig. 2.** Time evolution of diameter ($d$) or thickness ($t$) of different parts of BNP and of the whole BNP. The interfacial layer and the oxide/evaporation layer reach a dynamic equilibrium during Stage II.

Stage Ia can be considered as the pre-heating stage. As seen in Figs. 2 and 3, $t_{oxide/evaporation}$ increases with the rising temperature and reaches its maximum at the end of Stage Ia. It is worth mentioning that the temperature inside the BNP increases homogeneously as the temperature profile of each part of the BNP almost overlaps throughout the simulation. This phenomenon means that there is no significant heat transfer among different parts of the BNP. Central cross-sectional snapshots of the BNP at 0 and 0.21 ns show that the volume of the oxide/evaporation layer is accordingly expanded. Meanwhile, some chain-like oxides start to appear, which are ready for evaporation. A small number of ambient O species (including both molecular and atomic oxygen) are adsorbed on the BNP surface. During this stage, the B core further reacts with the oxide/evaporation layer as $t_{interfacial}$ is thickening, whereas $d_{core}$ is decreasing.

Stage Ib is the fast evaporation stage. At the beginning of this stage, $T_{oxide/evaporation}$ climbs to about 1970 K, from which the oxide/evaporation layer evaporates rapidly. Before this point, no significant weight loss of BNP is observed. This $T_{oxide/evaporation}$ is slightly lower than the normal boiling point of $B_2O_3$ (2133 K), which is reasonable because the boiling point of nano-sized particles could be lower due to the larger specific surface area compared with their bulk counterparts. During this stage, the whole BNP is covered by chain-like oxides and the oxides grow into longer chains before evaporation (see snapshot at 0.35 ns). Ambient O species are observed to penetrate into the interior of the oxide/evaporation layer as a result of the loose structure. Apparently, both $t_{oxide/evaporation}$ and $W_{BNP}$ drop dramatically. The B core continues to react with the oxide/evaporation layer as $t_{interfacial}$ and $d_{core}$ follow the same trend as in Stage Ia. The temperature rise is becoming slower, and $T_{BNP}$ reaches about 2900 K at the end of Stage Ib. The snapshot at 0.59 ns shows that only a thin oxide/evaporation layer with short chain oxides and few ambient O species covers on the BNP surface. Core B atoms are found to be included in this thin layer.

The combustion of the B core dominates the Stage II. Both $t_{interfacial}$ and $t_{oxide/evaporation}$ still increase slightly until about 1 ns with the rising temperature, after which $t_{interfacial}$ and $t_{oxide/evaporation}$ are stabilized at around 3 Å and $T_{BNP}$ is approximately kept at 3200 K. The higher final $T_{BNP}$ than the ambient temperature 3000 K is attributed to the heat release of combustion. According to the highly overlapped $t_{interfacial}$ and $t_{oxide/evaporation}$, the interfacial layer and the oxide/evaporation layer reach a dynamic equilibrium at Stage II. To be more specific, the consumption and generation of the interfacial layer and of the oxide/evaporation layer reach equilibrium, and are kept synchronized. Since $d_{core}$ keeps decreasing, the dynamically equilibrated interfacial and oxide/evaporation layers move towards the centre of the B core as a whole. It can be seen that increasingly more ambient O species participate in the reaction during this stage (see snapshots at 1.10 and 1.60 ns). In other words, the surface of BNP is continuously oxidized and then evaporated. This dynamic process drives the B core combustion during Stage II. In the meantime, the interfacial layer is maintained through the reaction of the B core with the oxide/evaporation layer. Consequently, $W_{BNP}$ steadily drops to about 55 % at the end of the simulation. Based on the weight loss curve, the total combustion time of the BNP can be estimated as 17.4 ns (see Fig. S5 in the Supplementary Material). As Stage I ends at 0.59 ns, the combustion time of the second stage is calculated as 16.81 ns. It is noticed that the ratio of the combustion time

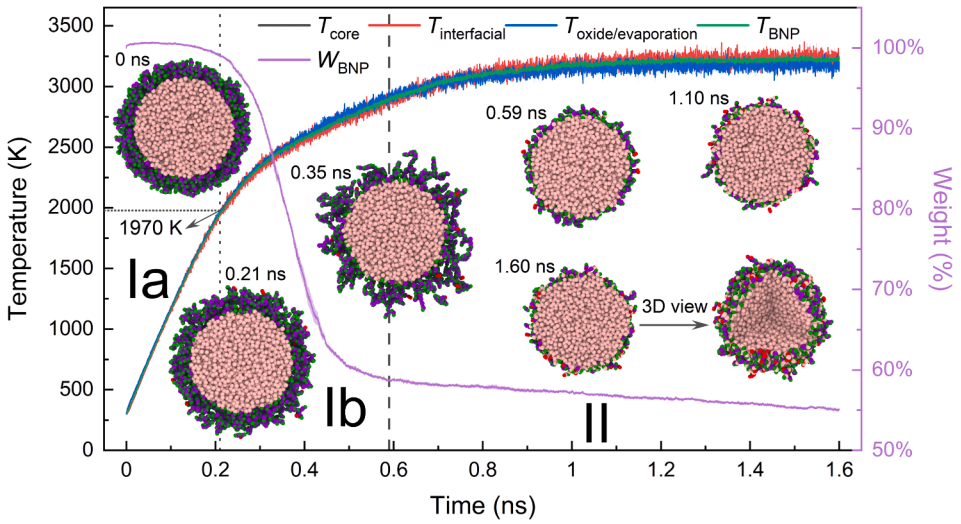


**Fig. 3.** Time evolution of temperature ($T$) of different parts of BNP and of the whole BNP, weight loss ($W$) curve of the BNP, and snapshots of the BNP at representative time points. $T_{core}$ is invisible as it is covered by the other lines. Atoms colouring scheme: core B – pink; shell B – purple; shell O – green; molecular oxygen O – red. (For interpretation of the references to color in this figure legend, the reader is referred to the web version of this article.)

between the second stage and the first stage evaluated in the present study (29) is larger than that obtained in previous experimental work (normally around 2 depending on different conditions) [3–6], which could mainly result from the thinner oxide layer and higher temperature employed in the MD simulation to circumvent the high computational cost. At the same temperature, the first stage is shorter if the BNP has a thinner oxide layer as its evaporation is faster. Considering the same second combustion stage, the ratio of the combustion time is larger. For scenarios of the same BNP under different temperatures, the combustion times of Stage I and II both become longer as the temperature decreases. The exact relationship between the combustion time ratio and the temperature needs further investigation. Other factors including ambient atmosphere and pressure, size of the nanoparticle, and measuring method that used in the experiment could also affect this time ratio.

### 3.2. Diffusion mechanism of BNP combustion

The diffusion mechanism of the BNP combustion is revealed in the present study. To study the diffusion of ambient oxygen, time evolution of the ratio ($R$) between number of ambient O atoms and of B atoms of each part of the BNP is plotted in Fig. 4a. The results are consistent with the snapshots shown in Fig. 3. Only a small number of ambient O species are adsorbed on the BNP surface during Stage Ia. As a result, $R_{oxide/evaporation}$ keeps constant at a very low level and $R_{interfacial}$ stays at zero. During Stage Ib of fast evaporation, ambient O species quickly flow into the interior of the oxide/evaporation layer because the chain-like oxides grows longer and the layer structure becomes looser, leading to a fast increase in $R_{oxide/evaporation}$. The growth in $R_{interfacial}$ is relatively moderate at this stage, which means ambient O species start to interact with the interfacial layer. From the beginning of Stage II, with the active participation of ambient O species, the remaining thin oxide/evaporation layer involves increasingly more ambient O atoms. Consequently, the number of O atoms in the interfacial layer formed by the reaction of the B core with the oxide/evaporation layer is also growing. Therefore, the steady increase in both $R_{oxide/evaporation}$ and $R_{interfacial}$ is presented during Stage II. It is obvious that nearly no ambient O species diffuse into the B core during the whole simulation as the oxidation reaction of the BNP only takes place on the BNP surface from Stage II and the B core is consumed layer by layer through evaporation of surface oxides. In general, the BNP evaporates by means of continuous evaporation of surface oxides, and the surface evaporation has significant effects on

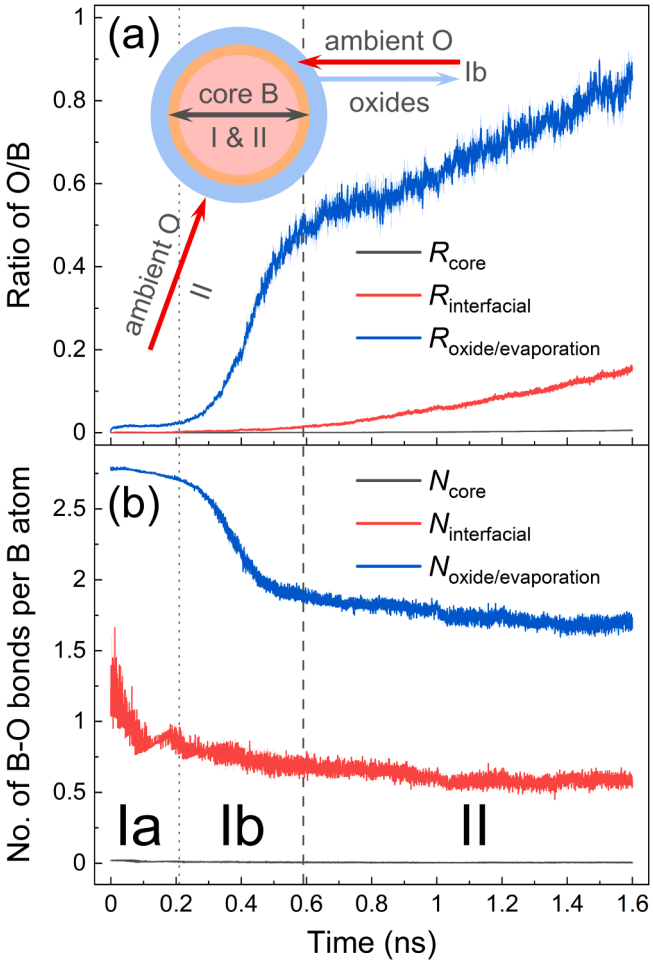


**Fig. 4.** Time evolution of (a) the ratio ($R$) between number of ambient O atoms and of B atoms of each part of the BNP, and (b) the number ($N$) of B-O bonds per B atom of each part of the BNP.

further oxidation of BNP during Stage II. This surface oxidation-evaporation reaction mode leads to inefficient combustion of BNP.

Time evolution of the number ($N$) of B-O bonds per B atom of each

part of the BNP is determined and presented in Fig. 4b, which provides insights into the composition information and oxidation state of each part. $N$ is counted based on each B atom. Taking a single $B_2O_3$ molecule as an example, each B atom has two B-O bonds, resulting in a $N$ of two. $N_{core}$ is basically zero owing to the absence of O atoms. The rapid temperature rise during Stage Ia promotes the reaction between the B core and the oxide/evaporation layer, leading to the fast decay of $N_{interfacial}$. In addition to the interfacial reaction, the expansion of the oxide/evaporation layer also contributes to the moderate decrease in $N_{oxide/evaporation}$. From Stage Ib, $N_{interfacial}$ reduces smoothly and tends to be stable after entering Stage II, during which the dynamic equilibrium of the interfacial layer and the oxide/evaporation layer is achieved. $N_{oxide/evaporation}$ experiences a rapid drop during evaporation as the amorphous oxides grow into long chains. Similarly, $N_{oxide/evaporation}$ is also gradually stabilized starting from Stage II. Overall, the oxidation state of the oxide/evaporation layer is always higher than that of the interfacial layer. Additionally, the low $N_{interfacial}$ value indicates that the interfacial layer is mainly consisted of B suboxides, whereas the equilibrated $N_{oxide/evaporation}$ value (slightly less than two) at Stage II demonstrates the incomplete oxidation of the oxide/evaporation layer that facilitates the surface reaction.

Combining with the results discussed in Section 3.1, to summarize, no ambient O species diffusion is observed at Stage Ia. The evaporation of oxides and diffusion of ambient O species into the oxide/evaporation layer proceed simultaneously during Stage Ib. From Stage II, excluding the gas phase reactions, ambient O species are only involved in the surface oxidation reaction of the BNP. The B core is free of ambient O species diffusion throughout the simulation. With regard to the BNP itself, the interfacial layer is maintained during the whole simulation, which is formed by the reaction of the B core with the oxide/evaporation layer. It can also be described as the diffusion of the core B atoms into the oxide/evaporation layer, which is mentioned in previous experimental studies of micron-sized B [2,11]. Additionally, the thickness of the interfacial layer is increased thus the diffusion of the core B atoms is enhanced with the elevated temperature. In brief, the reaction shifts from evaporation and diffusion dually controlled at Stage I to chemically controlled at Stage II.

### 3.3. Gas phase and surface reactions

Fig. 5 shows time evolution of the number of key gas phase $B_xO_y$ species (with a maximum number greater than 30) observed during the simulation and their main reaction pathways. No significant product formation is observed at the end of Stage Ia. The fast release of $B_xO_y$ species starts from Stage Ib as a result of the oxides evaporation. Specifically, the $B_xO_y$ detaches from the chain-like oxides to the gas phase. Various $B_xO_y$ species where $x > 4$ are also detected but they quickly decompose into smaller ones after leaving the oxide chain, leading to the five most remarkable $B_xO_y$ species as shown in Fig. 5a and 5b. In addition to $B_2O_3$, which is the ideal and main product of B combustion, $BO_2$ is found to be a dominant intermediate species. This finding agrees well with experimental results that $BO_2$ is observed and is an important intermediate species during the BNP combustion [4,6]. The number of $B_3O_4$, $B_4O_5$, and $B_4O_6$ reaches the peak and begins to decrease when the fast evaporation stage is about to finish, whereas the production of $BO_2$ and $B_2O_3$ keeps climbing to the end of the simulation. The main reaction pathways involving the listed key $B_xO_y$ species are (see Fig. 5c): R1) $B_4O_6 \rightarrow B_3O_4 + BO_2$; R2) $B_4O_5 \rightarrow B_3O_4 + BO$; R3) $B_3O_4 \rightarrow B_2O_3 + BO$; R4) $BO_2 + BO \rightarrow B_2O_3$. R1-R3 demonstrate the consumption ways of $B_3O_4$, $B_4O_5$, and $B_4O_6$. It can be seen that $B_3O_4$ is also a crucial intermediate, which acts as a bridge for the conversion of larger $B_xO_y$ species to $B_2O_3$. When the reaction proceeds to Stage II, the $B_xO_y$ released from the BNP are mainly $BO_2$ and $B_2O_3$ because the surface is covered by short chain oxides. As an active intermediate species, the number of $BO_2$ tends

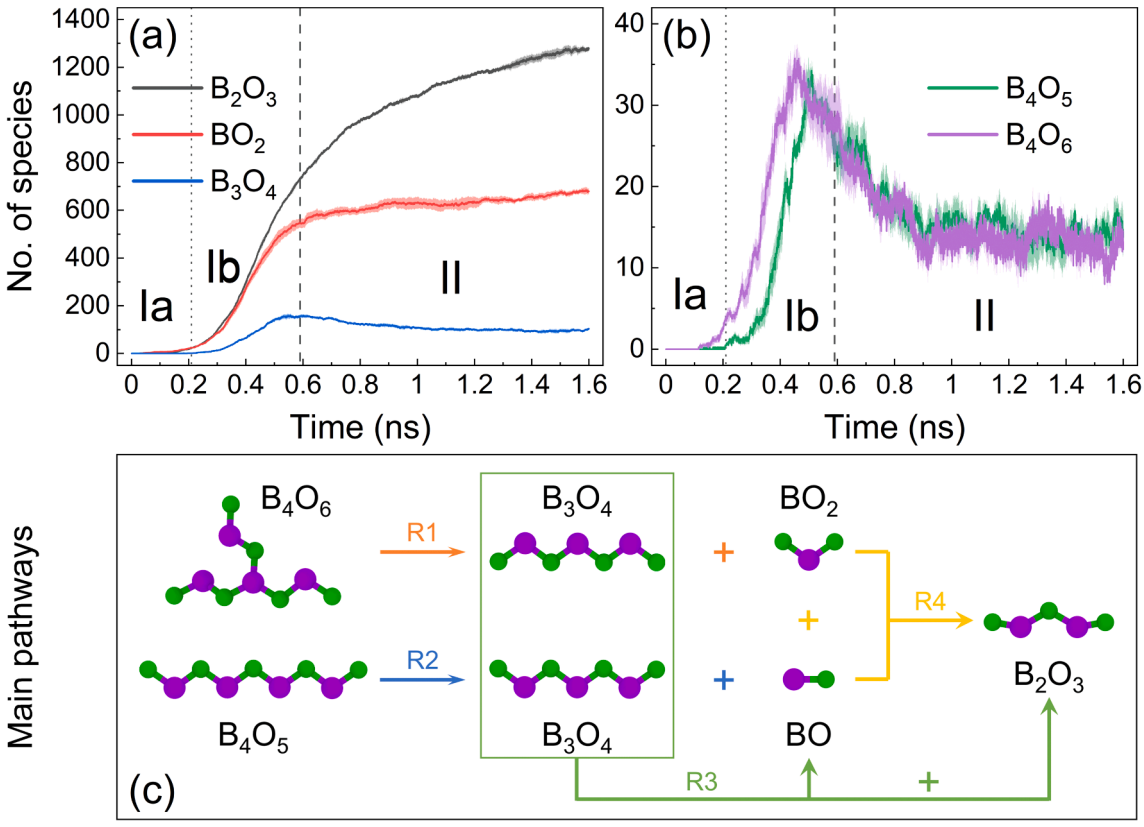


**Fig. 5.** Time evolution of the number of key gas phase $B_xO_y$ species observed during the simulation and their main reaction pathways. All $B_xO_y$ species, whose maximum number is greater than 30 are considered as key species. Atoms colouring scheme: B – purple; O – green. (For interpretation of the references to color in this figure legend, the reader is referred to the web version of this article.)

to be stable. Both the direct release from the BNP surface and gas phase reactions contribute to the significant $B_2O_3$ production.

The interaction between $O_2$ and the BNP during Stage II is tracked to understand the surface reactions. It is observed that when a $O_2$ molecule approaches the surface, it endeavours to seek for a B atom, which is only bonded to B with no bonding O atoms. Once such a B atom is found, the $O_2$ molecule is first adsorbed on this B atom. Subsequently, the O-O bond is broken and the two O atoms are able to move freely on the surface. The adsorbed $O_2$ is finally become part of the oxide/evaporation layer and participate in the aforementioned combustion reactions.

## 4. Conclusions

We perform the ReaxFF MD simulations to investigate the fundamental combustion mechanisms of BNP. The experimentally observed two-stage combustion is reproduced in the present study. The results show that the first stage (I) is further divided into the pre-heating stage (Ia) and the fast evaporation stage (Ib). During Stage Ia, the volume of the oxide/evaporation layer is expanded and some chain-like oxides appear. Meanwhile, the B core further reacts with the oxide/evaporation layer. From Stage Ib, the oxide/evaporation layer evaporates rapidly and the oxides grow into longer chains before evaporation. The B core continues to react with the oxide/evaporation layer. Stage II is dominated by the combustion of the B core, during which the interfacial layer and the oxide/evaporation layer are found to reach a dynamic equilibrium. The surface of BNP is continuously oxidized and then evaporated. This dynamic process drives the B core combustion, resulting in a steady mass drop of the BNP. The diffusion mechanism of the BNP combustion is revealed. The evaporation of oxides and diffusion of ambient O species into the oxide/evaporation layer proceed simultaneously during Stage Ib, while ambient O species are only involved in the surface oxidation reaction of the BNP in Stage II excluding the gas phase reactions. No ambient O species diffusion into the B core is observed but the diffusion of the core B atoms into the oxide/evaporation layer occurs throughout the simulation. Additionally, the diffusion of the core B atoms is enhanced with the elevated temperature. To summarize, the reaction shifts from evaporation and diffusion dually controlled at Stage I to chemically controlled at Stage II. It is found that $B_xO_y$ detaches from the chain-like oxides to the gas phase during evaporation. In addition to the main combustion product $B_2O_3$, $BO_2$ is a dominant intermediate species, which agrees well with experimental observations. Furthermore, $B_3O_4$ is found to be an important intermediate, which bridges the conversion of larger $B_xO_y$ species to $B_2O_3$.

The present study reveals the detailed microscopic evolution of each stage, the diffusion mechanism, and the dominant intermediate species together with their reaction pathways of the BNP combustion, which facilitates fundamental understanding. Based on the findings obtained from our study, it can be concluded that the better combustion characteristics of nano-sized B than those of micron-sized B (excluding the effects of agglomeration of nanoparticles) could be attributed to the more efficient evaporation of the oxide layer at the nanoscale. Compared with micron-sized B, the subsequent B core combustion is also accelerated due to the well-known advantages of nanoparticles. The new atomistic insights into the combustion of BNP provided in the present research could potentially benefit the design and practical application of nano-sized B as additives for high-energy fuels.

## CRediT authorship contribution statement

**Muye Feng:** Writing – original draft, Visualization, Validation, Methodology, Formal analysis, Data curation, Conceptualization. **Yi Wang:** Visualization, Methodology, Formal analysis, Data curation. **Dingyu Hou:** Writing – original draft, Validation, Investigation. **Heping Li:** Validation, Investigation, Conceptualization. **Kai H. Luo:** Writing – review & editing, Supervision, Resources, Project administration, Funding acquisition. **Xuefei Xu:** Writing – review & editing, Validation, Supervision, Resources, Project administration, Investigation.

## Declaration of competing interest

The authors declare that they have no known competing financial interests or personal relationships that could have appeared to influence the work reported in this paper.

## Data availability

Data will be made available on request.

## Acknowledgements

Funding from the National Natural Science Foundation of China (Grant No. 52106164) and the UK Engineering and Physical Sciences Research Council (Grant Nos. EP/T015233/1 and EP/X035875/1) is gratefully acknowledged. This work made use of computational support by CoSeC, the Computational Science Centre for Research Communities, through UKCOMES.

## Appendix A. Supplementary material

Supplementary data to this article can be found online at https://doi.org/10.1016/j.fuel.2024.132628.

## References

[1] Ojha PK, Karmakar S. Boron for liquid fuel engines-A review on synthesis, dispersion stability in liquid fuel, and combustion aspects. Prog Aerosp Sci 2018;100:18–45.
[2] Yeh CL, Kuo KK. Ignition and combustion of boron particles. Prog Energy Combust Sci 1996;22(6):511–41.
[3] Song Q, Cao W, Wei X, Liu J, Yuan J, Li X, et al. Laser ignition and combustion characteristics of micro- and nano-sized boron under different atmospheres and pressures. Combust Flame 2021;230:111420.
[4] Young G, Sullivan K, Zachariah MR, Yu K. Combustion characteristics of boron nanoparticles. Combust Flame 2009;156(2):322–33.
[5] Yu D, Kong C, Zhuo J, Yao Q, Li S, Wang M, et al. Combustion characteristics of well-dispersed boron submicroparticles and plasma effect. Combust Flame 2018;188:94–103.
[6] Acharya S, Karmakar S, Dooley KM. Ignition and combustion of boron nanoparticles in ethanol spray flame. J Propuls Power 2012;28(4):707–18.
[7] Macek A, Semple JM. Combustion of boron particles at atmospheric pressure. Combust Sci Technol 1969;1(3):181–91.
[8] Haynes WM. CRC Handbook of Chemistry and Physics. CRC Press; 2014.
[9] King MK. Ignition and combustion of boron particles and clouds. J Spacecr Rockets 1982;19(4):294–306.
[10] Glassman I, Williams FA, Antaki P. A physical and chemical interpretation of boron particle combustion. Symp Combust 1985;20(1):2057–64.
[11] Liang D, Liu J, Zhou Y, Zhou J, Cen K. Ignition delay kinetic model of boron particle based on bidirectional diffusion mechanism. Aerosp Sci Technol 2018;73:78–84.
[12] Liang D, Shen D, Zhong W, Wang Y, Liu J. Nuclear shell model for the ignition process of boron particle with binary surface oxide layer. Combust Flame 2021;225:320–8.
[13] Wang J, Zhu B, Sun Y. Microscopic mechanism of α-rhombic crystal boron nanocluster oxidation in oxygen. Fuel 2022;310:122448.
[14] Senftle T, Hong S, Islam MM, Kylasa SB, Zheng Y, Shin YK, et al. The ReaxFF reactive force-field: Development, applications, and future directions. Npj Comput Mater 2016;2:15011.
[15] Ashraf C, van Duin ACT. Extension of the ReaxFF combustion force field toward syngas combustion and initial oxidation kinetics. J Phys Chem A 2017;121(5):1051–68.
[16] Feng M, Jiang XZ, Luo KH. A reactive molecular dynamics simulation study of methane oxidation assisted by platinum/graphene-based catalysts. Proc Combust Inst 2019;37:5473–80.
[17] Feng M, Jiang XZ, Zeng W, Luo KH, Hellier P. Ethanol oxidation with high water content: A reactive molecular dynamics simulation study. Fuel 2019;235:515–21.
[18] Feng M, Jiang XZ, Mao Q, Luo KH, Hellier P. Initiation mechanisms of enhanced pyrolysis and oxidation of JP-10 (exo-tetrahydrodicyclopentadiene) on functionalized graphene sheets: Insights from ReaxFF molecular dynamics simulations. Fuel 2019;254:115643.
[19] Jiang XZ, Feng M, Zeng W, Luo KH. Study of mechanisms for electric field effects on ethanol oxidation via reactive force field molecular dynamics. Proc Combust Inst 2019;37:5525–35.

[20] Chu Q, Shi B, Liao L, Luo KH, Wang N, Huang C. Ignition and oxidation of core–shell Al/$Al_2O_3$ nanoparticles in an oxygen atmosphere: Insights from molecular dynamics simulation. J Phys Chem C 2018;122(51):29620–7.
[21] Feng M, Li H, Mao Q, Luo KH, Hellier P. Fundamental study on mechanisms of thermal decomposition and oxidation of aluminum hydride. J Phys Chem C 2019; 123(40):24436–45.
[22] Hong S, van Duin ACT. Atomistic-scale analysis of carbon coating and its effect on the oxidation of aluminum nanoparticles by ReaxFF-molecular dynamics simulations. J Phys Chem C 2016;120(17):9464–74.
[23] Feng M, Li H, Luo KH. A molecular dynamics study on oxidation of aluminum hydride ($AlH_3$)/hydroxyl-terminated polybutadiene (HTPB) solid fuel. Proc Combust Inst 2021;38:4469–76.
[24] Plimpton S. Fast parallel algorithms for short-range molecular dynamics. J Comput Phys 1995;117(1):1–19.
[25] Weismiller MR, van Duin ACT, Lee J, Yetter RA. ReaxFF reactive force field development and applications for molecular dynamics simulations of ammonia borane dehydrogenation and combustion. J Phys Chem A 2010;114(17):5485–92.
[26] Stukowski A. Visualization and analysis of atomistic simulation data with OVITO–the Open Visualization Tool. Model Simul Mater Sci Eng 2009;18(1): 15012.
[27] Ao W, Zhou JH, Yang WJ, Liu JZ, Wang Y, Cen KF. Ignition, combustion, and oxidation of mixtures of amorphous and crystalline boron powders. Combust Explos Shock Waves 2014;50(6):664–9.
[28] Hashim SA, Karmakar S, Roy A. Combustion characteristics of boron-HTPB-based solid fuels for hybrid gas generator in ducted rocket applications. Combust Sci Technol 2019;191(11):2082–100.